

# Microfluidic Generation of Thin-Shelled Polyethylene Glycol-Tyramine Microgels for Non-Invasive Delivery of Immunoprotected $\beta$ -Cells


Nuno Araújo-Gomes,\* Barbara Zoetebier-Liszka, Bas van Loo, Malin Becker, Suzanne Nijhuis, Alexandra M. Smink, Bart J. de Haan, Paul de Vos, Marcel Karperien, and Jeroen Leijten\*

Transplantation of microencapsulated pancreatic cells is emerging as a promising therapy to replenish  $\beta$ -cell mass lost from auto-immune nature of type I diabetes mellitus (T1DM). This strategy intends to use micrometer-sized microgels to provide immunoprotection to transplanted cells to avoid chronic application of immunosuppression. Clinical application of encapsulation has remained elusive due to often limited production throughputs and body's immunological reactions to implanted materials. This article presents a high-throughput fabrication of monodisperse, non-immunogenic, non-degradable, immunoprotective, semi-permeable, enzymatically-crosslinkable polyethylene glycol-tyramine (PEG-TA) microgels for  $\beta$ -cell microencapsulation. Monodisperse  $\beta$ -cell laden microgels of  $\approx 120 \mu\text{m}$ , with a shell thickness of  $20 \mu\text{m}$  are produced using an outside-in crosslinking strategy. Microencapsulated  $\beta$ -cells rapidly self-assemble into islet-sized spheroids. Immunoprotection of the microencapsulated is demonstrated by inability of FITC-IgG antibodies to diffuse into cell-laden microgels and NK-cell inability to kill microencapsulated  $\beta$ -cells. Multiplexed ELISA analysis on live blood immune reactivity confirms limited immunogenicity. Microencapsulated MIN6 $\beta$ 1 spheroids remain glucose responsive for 28 days in vitro, and able to restore normoglycemia 5 days post-implantation in diabetic mice without notable amounts of cell death. In short, PEG-TA microgels effectively protect implanted cells from the host's immune system while being viable and functional, validating this strategy for the treatment of T1DM.

in an inability to regulate systemic blood glucose levels. T1DM often has its onset in children and young adults and accounts for  $\approx 10\%$  of the total cases of diabetes mellitus, and its prevalence continues to rise. Due to its significant morbidity and mortality, T1DM places a heavy burden on both diabetic individuals and healthcare systems. Conventional treatments for T1DM (e.g., daily insulin administration) have adverse effects such as life threatening hypoglycemia<sup>[1]</sup> and frequent hyperglycemia that can lead to diabetic complications such as heart failure,<sup>[2]</sup> allergic reactions,<sup>[3]</sup> weight gain,<sup>[4]</sup> lipodystrophy,<sup>[5]</sup> and hypokalemia.<sup>[6]</sup> These current drawbacks can be prevented by providing patients with an insulin-producing cell-source that regulates glucose levels on a minute-to-minute level. To accomplish this, various novel experimental treatments based on immunotherapy, implantable devices, and cell therapy are under investigation. In particular, transplantation of pancreatic islet and  $\beta$ -cell transplantation has emerged as a promising regenerative therapeutic approach as it can replenish the lost  $\beta$ -cell mass. However, poor survival and function of transplanted cells, lack of sufficient human donors, and need for immunosuppressive drugs to evade the host's allo- and auto-immune response has prevented this otherwise promising strategy from becoming a routine clinical reality.<sup>[7]</sup>

## 1. Introduction

Type I diabetes (T1DM) is an auto-immune disease that results in the destruction of insulin-producing  $\beta$ -cells, which results

 The ORCID identification number(s) for the author(s) of this article can be found under <https://doi.org/10.1002/adhm.202301552>

© 2023 The Authors. Advanced Healthcare Materials published by Wiley-VCH GmbH. This is an open access article under the terms of the Creative Commons Attribution License, which permits use, distribution and reproduction in any medium, provided the original work is properly cited.

DOI: 10.1002/adhm.202301552

N. Araújo-Gomes, B. Zoetebier-Liszka, B. van Loo, M. Becker, S. Nijhuis, M. Karperien, J. Leijten  
Department of Developmental BioEngineering, TechMed Centre  
University of Twente  
Drienerlolaan 5, Enschede 7522NB, The Netherlands  
E-mail: n.gomes@utwente.nl jeroen.leijten@utwente.nl  
A. M. Smink, B. J. de Haan, P. de Vos  
Department of Pathology and Medical Biology, Section of Immunoen-  
docrinology  
University of Groningen, University Medical Center Groningen  
Hanzeplein 1, Groningen 9713 GZ, The Netherlands

Semipermeable hydrogel networks can be designed to prevent diffusion of  $\beta$ -cell destructive antibodies, while allowing for diffusion of smaller molecules (e.g., metabolites, waste products, and growth factors) based on size exclusion.<sup>[8]</sup> Semipermeable hydrogels therewith possess the potential to offer transplanted (e.g., allogeneic or xenogeneic) cells an immunoprotective membrane that enables their long-term survival and function in an immunosuppression-free manner.<sup>[7c,9]</sup> The type of cell-laden biomaterials used for these approaches represent a next generation of biomaterials specifically aimed at mitigating uncontrolled immunological processes, appropriately named immunomodulatory materials.<sup>[10]</sup> In particular, immunoprotective micrometer-sized hydrogels, named microgels, have been explored owing to their minimal diffusive lengths between the host's blood vessels and the implanted  $\beta$ -cells (<100  $\mu\text{m}$ ). Various microgels composed of amongst others alginate,<sup>[7c]</sup> agarose,<sup>[11]</sup> poly(vinyl alcohol) (PVA),<sup>[12]</sup> and polyethylene glycol (PEG)<sup>[13]</sup> have been investigated. Despite promising results, which show extended survival times of >1 year, these microgels often associate with cell-damaging fabrication processes (e.g., UV-induced crosslinking),<sup>[14]</sup> degradation over time (e.g., loss of divalent ions in ionically crosslinked systems),<sup>[15]</sup> poor control over fabrication process (e.g., batch-to-batch production and/or reliance on natural biomaterials with biological variability),<sup>[16]</sup> and lack of function improving cell-to-cell contacts between  $\beta$ -cells (e.g.,  $\beta$ -cells suspended in solid microgels).<sup>[17]</sup> An ideal microgel material to deliver and immunoprotect  $\beta$ -cells has thus remained elusive.

Therefore, the key objective of this manuscript is to develop and introduce a cytocompatible microfluidic production strategy to generate non-degradable and immunoprotective microcapsules, which could act as a viable alternative for  $\beta$ -cell transplantation strategies, capable of delivering insulin continuously to the living host.

For that, we present the microfluidic generation of monodisperse, cytocompatible, enzymatically crosslinked, hollow, thin-shelled, non-degradable, immunoprotective, PEG microgels with the aim to be used for cell-encapsulation for the treatment of T1DM. Specifically, we conjugated eight-arm PEG with tyramine (TA) moieties (PEG-TA), which when flown through a flow focus microfluidic droplet generator allowed for delayed outside-in crosslinking, which produced micrometer thin-shelled hollow microgels. When  $\beta$ -cells were mixed into the polymer solution, cells autonomously self-assembled within the microgels to form islet-sized  $\beta$ -cell spheroids. A low-immunogenic PEG-TA microcapsule formulation was identified that, when laden with allogeneic  $\beta$ -cell spheroids, was capable of restoring normoglycemia in streptozotocin (STZ)-induced diabetic mice.

## 2. Results and Discussion

### 2.1. Hydrogels Fabrication via Enzymatic Crosslinking and Their Characterization

For the engineering of the immunoprotective microgels, PEG was selected as the biomaterial of choice owing to its high water content, low degradability, compatibility with cytocompatible/mild solvents, low biofouling, and potential immunoprotective properties.<sup>[18]</sup> To allow for its enzymatic crosslinking, an

eight-arm PEG backbone was functionalized (Figure 1a) with TA moieties. The final product (PEG-TA) was successfully functionalized with a degree of substitution (DS%) of 87%–100%, based on the corresponding H-NMR (nuclear magnetic resonance) spectrum (Figure 1b).

The introduction of phenol groups allowed for intermolecular TA–TA coupling via covalent carbon-carbon and carbon-oxygen bonds when exposed to horseradish peroxidase (HRP) and hydrogen peroxide to form stable hydrogel networks (Figure 1c). Lower PEG-TA concentrations (e.g., 2.5% and 5%) were associated with hydrogel contraction upon crosslinking, which resulted in relatively higher polymer content within the produced hydrogels as compared to their respective original precursor solution (Figure 1d). Lower availability of TA groups within the 2.5% and 5% polymer precursor solutions are likely to result in more interconnected networks, thus resulting in the repelling of solvent. In contrast, the 10% PEG-TA precursor solution was shaped stable as no contraction during crosslinking was observed. Rheological analysis of the formed hydrogel discs revealed an increase in the linear viscoelastic region (LVER) with higher frequency and strain regimes at higher polymer concentrations (Figure 1e,f). This can be attributed to a more entangled network with only partially bound polymers being able to dissipate energy during strain. The dynamic moduli of hydrogels within the LVER showed an increase with increasing polymer concentration (Figure 1g), resulting in storage moduli of  $\approx 3900$ ,  $\approx 9400$ ,  $\approx 11\,500$  Pa for 2.5%, 5%, and 10% polymer fraction, respectively.

### 2.2. Microfluidic Production of Enzymatically Crosslinked Immunoprotective Hollow PEG-TA Microgels

To produce hollow PEG-TA microgels, we leveraged a recently developed microfluidic device.<sup>[19]</sup> This platform is based on a flow focus microdroplet generation in the dripping regime followed by in-line enzymatic crosslinking of polymer's TA conjugates (Figure 2a). On-chip enzymatic crosslinking was chosen as it has consistently been reported to outperform conventional on-chip crosslinking strategies such as UV-initiated or ionic crosslinking in terms of cell survival and subsequent cell function.<sup>[20]</sup> Specifically, monodisperse PEG-TA microdroplets were produced by flowing PEG-TA solution through a polymethylmethacrylate (PMMA) microfluidic chip with a T-junction, with two inlets (polymer and oil at a 1:5 ratio with a flow speed  $96\ \mu\text{L}\ \text{min}^{-1}$ ), and one droplet outlet (Figure 2b). These microdroplets were subsequently flown off-chip within a silicon tube that was emersed in a hydrogen peroxide bath, which allowed the polymer's TA groups to be crosslinked via outside-in diffusion of hydrogen peroxide molecules, which formed monodisperse PEG-TA microgels (Figure 2c). The hollowness of the produced microgels was confirmed using focus ion beam scanning electron microscopy (FIB-SEM) (Figure 2d). TA–TA bonds of microgels were stained using ethidium homodimer-1 and visualized using fluorescent confocal microscopy, which revealed that the microgels' core measured  $\approx 120\ \mu\text{m}$  with a homogenous shell thickness of  $\approx 20\ \mu\text{m}$  (Figure 2e). Fabricating microgels with such small dimensions and thin shells was anticipated to ensure optimal diffusion of oxygen, nutrient, and insulin to and from encapsulated cells.

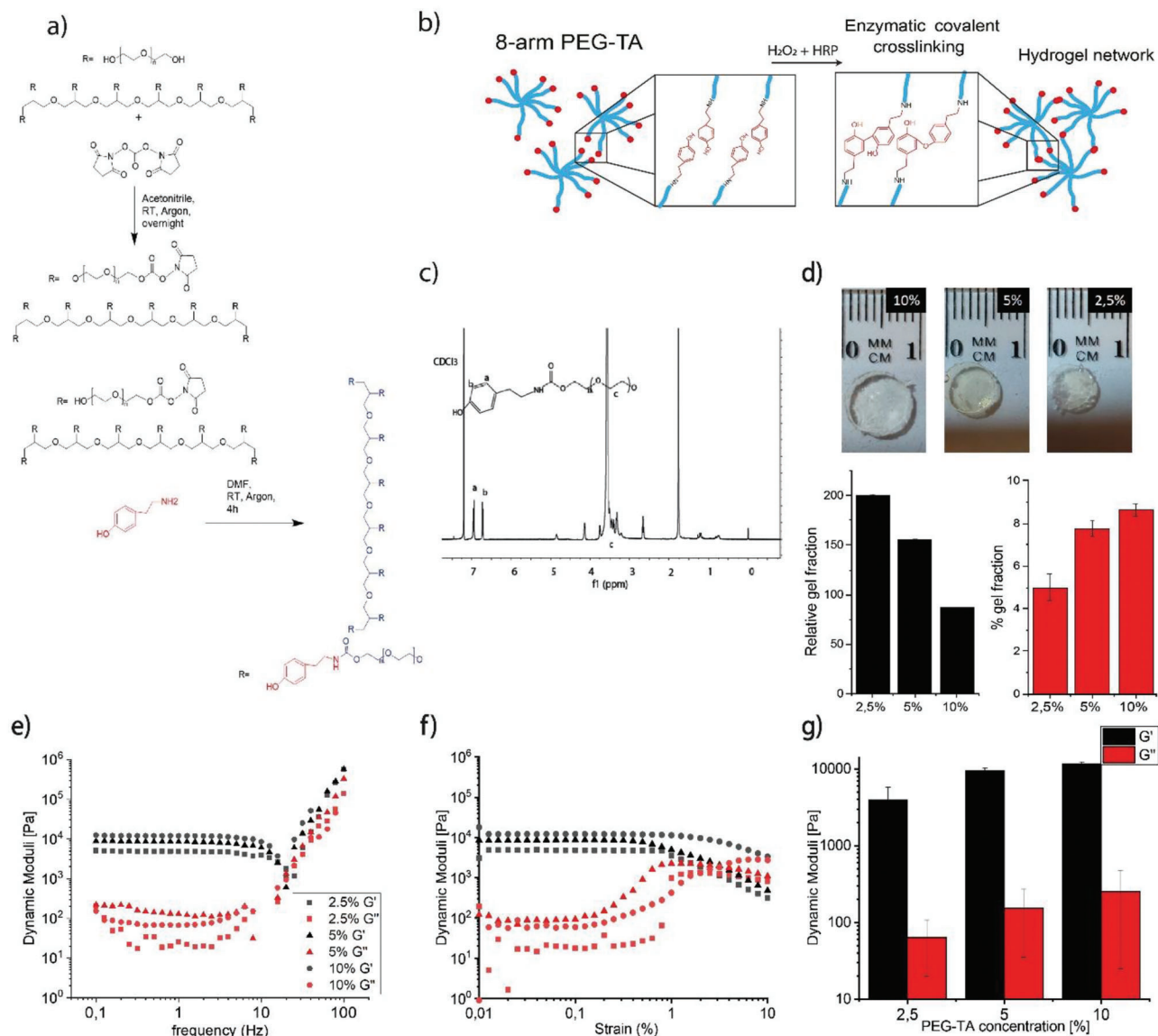


**Figure 1.** Synthesis and characterization of PEG-TA hydrogels. a) Schematic representation of PEG-TA synthesis. b)  $^1\text{H-NMR}$  spectrum of functionalized PEG-TA. c) Schematic depiction of the enzymatic crosslinking of PEG-TA hydrogel. d) Photographs of swollen hydrogels composed of 2.5%, 5%, and 10% of PEG-TA, and the corresponding percentages of total and relative gel fraction of the various concentrations of PEG-TA hydrogels. e) Rheological analysis using frequency sweeps and f) strain regimes, and the corresponding g) dynamic moduli (storage and loss) of various concentrations of PEG-TA hydrogel.

Rheologic analysis of the hollow microgels using interferometry-based nanoindentation revealed that the shell of the produced hollow microgels possessed a stiffness of  $\approx 20$  kPa for 5% PEG-TA and  $\approx 30$  kPa for 10% PEG-TA, while 2.5% PEG-TA microgels proved too soft to be accurately measured (Figure 2f). This difference is attributable to the distinct number of crosslinked groups in each condition. The range of stiffnesses obtained is well within the range of the elasticities found in most native biological tissues.<sup>[21]</sup> Although the inert (e.g., non-adhesive) nature of PEG-TA is unlikely to impact cellular behavior, stiffer (e.g., more densely crosslinked) materials are associated with increased long-term stability (e.g., prolonged degradation rates).<sup>[22]</sup>

The immunoprotective character of the produced microgels was assessed by measuring the permeability of the distinct microgel formulations (2.5–10% w/v) through incubation with FITC-labeled proteins of several molecular weights (MW from 10 kDa to 500 kDa), with additional diffusion studies of BSA (66.5 kDa) and IgG (150 kDa) (Figure 2g). Microgels composed of 10% PEG-TA (20 kDa) were proven to most effectively inhibit IgG diffusion while allowing for diffusion of BSA. This confirmed that continuous on-chip microfluidic production of PEG-TA microgels with a semi-permeable character that offered robust immunoprotection while allowing for the diffusion of smaller molecules such as oxygen, nutrients, growth factors, glucose, and insulin could be achieved (Figure 2h).



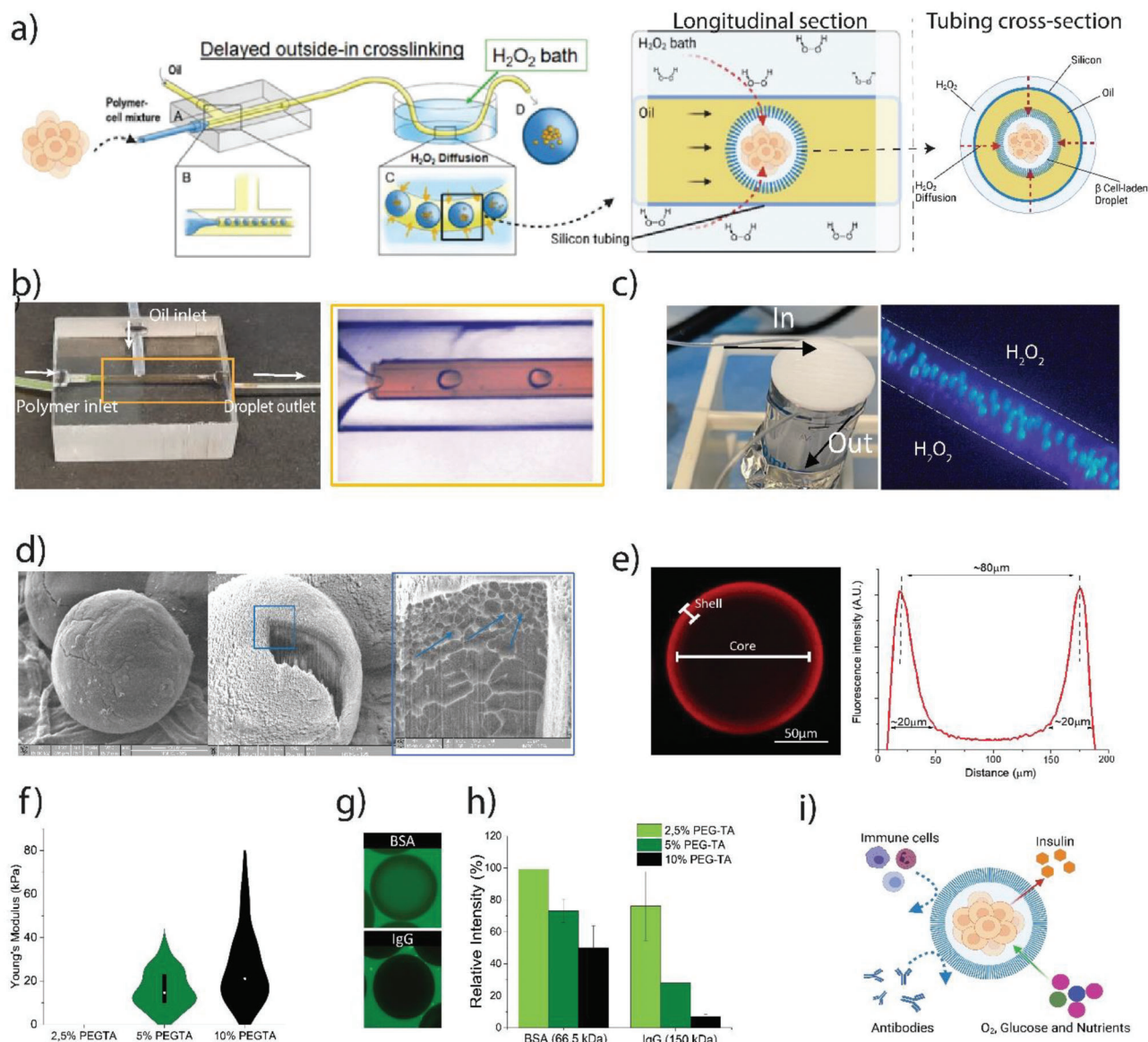


**Figure 2.** Microfluidic generation of enzymatically crosslinked immunoprotective hollow PEG-TA microgels. a) Schematic depiction of the microfluidic droplet generator and the delayed outside-in crosslinking strategy used to produce hollow microgels. b) Photograph of the polymethylmethacrylate microfluidic 3D glass capillary device in which micrometer-sized droplet are generated using a flow-focus nozzle arrangement. c) After their formation, the droplets are flown away from the chip into a silicone tube. This tube is submerged in a bath of diluted hydrogen peroxide, which facilitates the diffusion of hydrogen peroxide into the droplets. As a result, hollow microgels named microcapsules are formed. d) SEM microphotographs depicting 1) an intact microgel, 2) partially open microgel where its visible shell and hollow core. Amplification photographs show the semi-porous character of the microgel shell, indicated by the blue arrows. e) Fluorescence confocal micrograph displaying a microgel stained with EthD-1, highlighting its hollow structure. The corresponding histogram of the produced microgels showcases the visible presence of their empty compartments. The quantification was performed by analyzing the capsules along their equatorial plane. f) Young's modulus for the three tested formulations. g) Fluorescence confocal microphotographs and h) permeability study of the distinct microgel formulations after incubation with FITC-labelled BSA (MW: 66.5 kDa) and IgG (MW: 150 kDa). i) Schematic depiction of produced microgels highlighting the inherent ability to be impermeable to larger size molecules and immune cells while being permeable to small molecules such as insulin and glucose.

### 2.3. Characterization of Immune Responses to Hollow PEG-TA Microgels

To test the immunogenic profile of the produced hollow immunoprotective microgels, multiplex ELISA was performed on whole blood that was incubated with microgels composed

of 2.5%, 5%, and 10% PEG-TA (Figure 3a). An inverse dose-dependency of inflammatory profile in response to PEG-TA concentration was observed with 10% PEG-TA eliciting the lowest pro-inflammatory cytokine release (Figure 3b). To further investigate the potential difference in immunogenicity, we exposed monocytes (e.g., PMA-differentiated THP1 cells) to

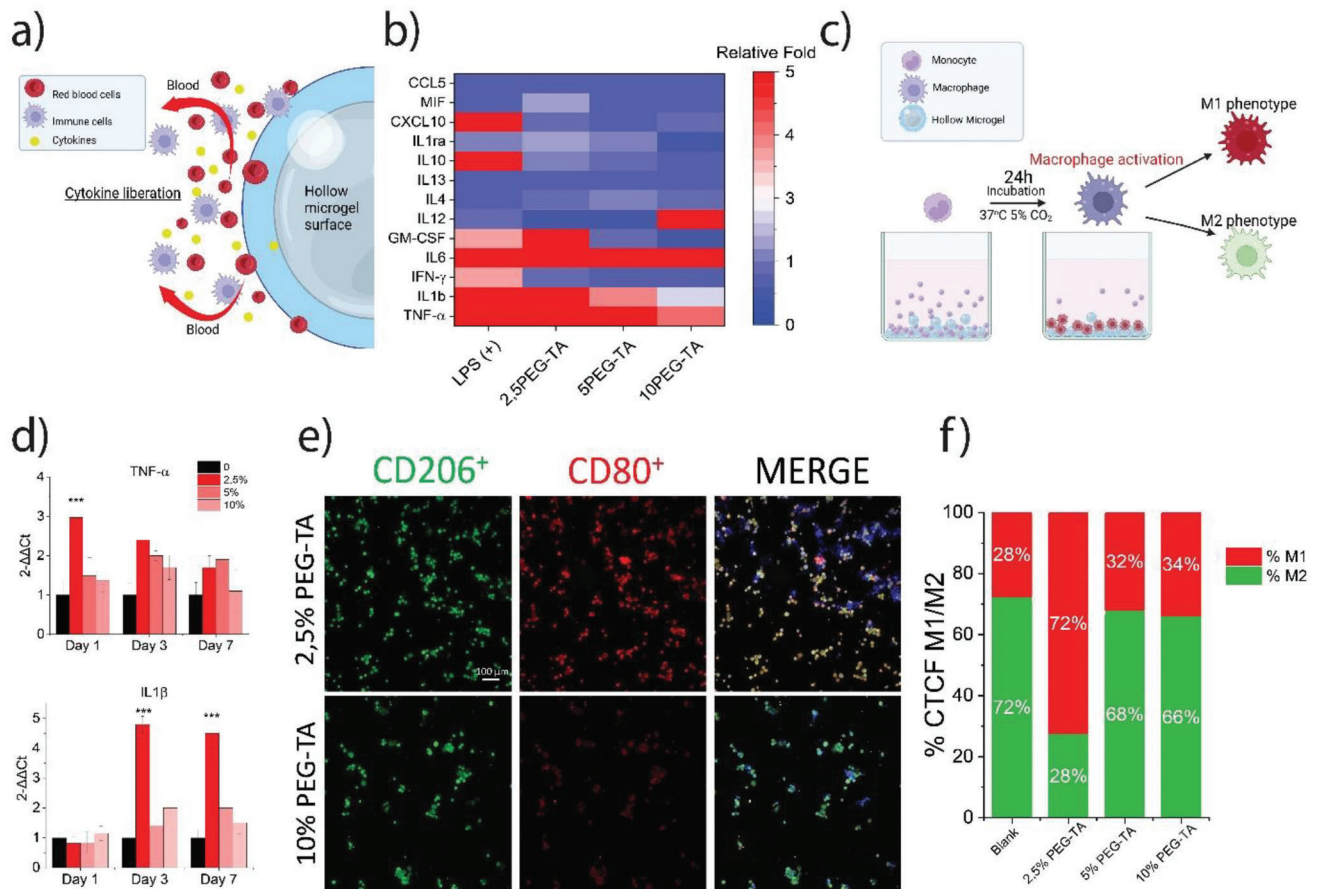


**Figure 3.** Assessment of in vitro immunogenicity of PEG-TA hollow microgels. a) Schematic depicting the whole blood experiment to determine the microgel's effect on cytokine secretion, and b) respective heatmap depicting inflammatory cytokine release profile after incubation with the distinct hollow microgel formulations after 7 days of incubation.  $N = 3$ . LPS ( $100 \text{ ng mL}^{-1}$ ) was used as a positive control for inflammation and saline buffer (HBSS) was used as a negative control. c) Schematic depiction of the experimental design for macrophage activation analysis and macrophage plasticity. d) Gene expression profile of pro-inflammatory cytokines TNF- $\alpha$  and IL1 $\beta$  of activated monocytes co-cultured with 2.5%, 5%, or 10% PEG-TA microgels. Relative mRNA expression was determined by RT-qPCR after 1, 3, and 7 days of culture and normalized to the housekeeping gene GAPDH. \*\*\*, one-way ANOVA  $p < 0.001$ . Data shown is representative of 3 biological samples pooled and 9 technical replicates were performed for each time point. e) Fluorescent microphotographs of PMA-differentiated macrophages co-cultured with 2.5% and 10% PEG-TA hollow microgels immunohistochemically stained for CD206 and CD80 after 7 days of microgel exposure. f) Relative corrected total cell fluorescence (CTCF) % of the M1 and M2 markers used. One-way ANOVA \*\*\*  $p < 0.001$ ,  $N = 3$  wells, quantification done based on 5 pictures per well.

hollow microgels composed of 2.5%, 5%, or 10% PEG-TA, and investigated their polarization into either a pro-inflammatory M1 or a pro-regenerative M2 phenotype over a culture period of 7 days (Figure 3c). Gene expression analysis of PMA-differentiated THP1 cells incubated in vitro with hollow microgels corroborated the inverse correlation between PEG-TA concentration and immunogenicity as RT-qPCR data revealed that 10% PEG-TA consistently associated with significantly lower TNF $\alpha$  and IL1 $\beta$  mRNA levels than 2.5% PEG-TA microgels (Figure 3d). Immunofluorescent analysis confirmed that while of cells exposed to 2.5% PEG-TA microgels for 7 days showed both increased expression of CD80 (e.g., M1 marker) and CD206 (e.g., M2 marker), 10% PEG-TA microgels associated with lowered expression of CD80 and increased expression of CD206 (Figure 3e,f).

Overall, microfluidic generation of PEG-TA microgels was demonstrated in a clean, easy, and highly-controllable manner

without the need for complex microfabrication technologies and dedicated infrastructures.<sup>[23]</sup> Moreover, the delayed crosslinking nature of the microdevice avoids direct crosslinking of the polymer on the droplet generator, reducing the device failure due to crosslinking-mediated channel clogging.

Depending on the final application, the versatile, inert, and cytocompatible character of PEG offers key advantages for  $\beta$ -cell delivery in comparison to other types of natural and synthetic polymers suitable for enzymatic crosslinking (e.g., modified alginate, silk, gelatin, or PVA), including reduced degradability, high water content, short diffusion rates, and low surface protein fouling.<sup>[15]</sup> This allows for reduction of the tissue fibrotic response and high nutrient availability for the encapsulated cells, thus decreasing the chance of implant failure.

Moreover, the micrometer-thin PEG-TA shell of the hollow microgel offered immunoprotection, while allowing for efficient diffusion of nutrients, waste products, and insulin with minimal



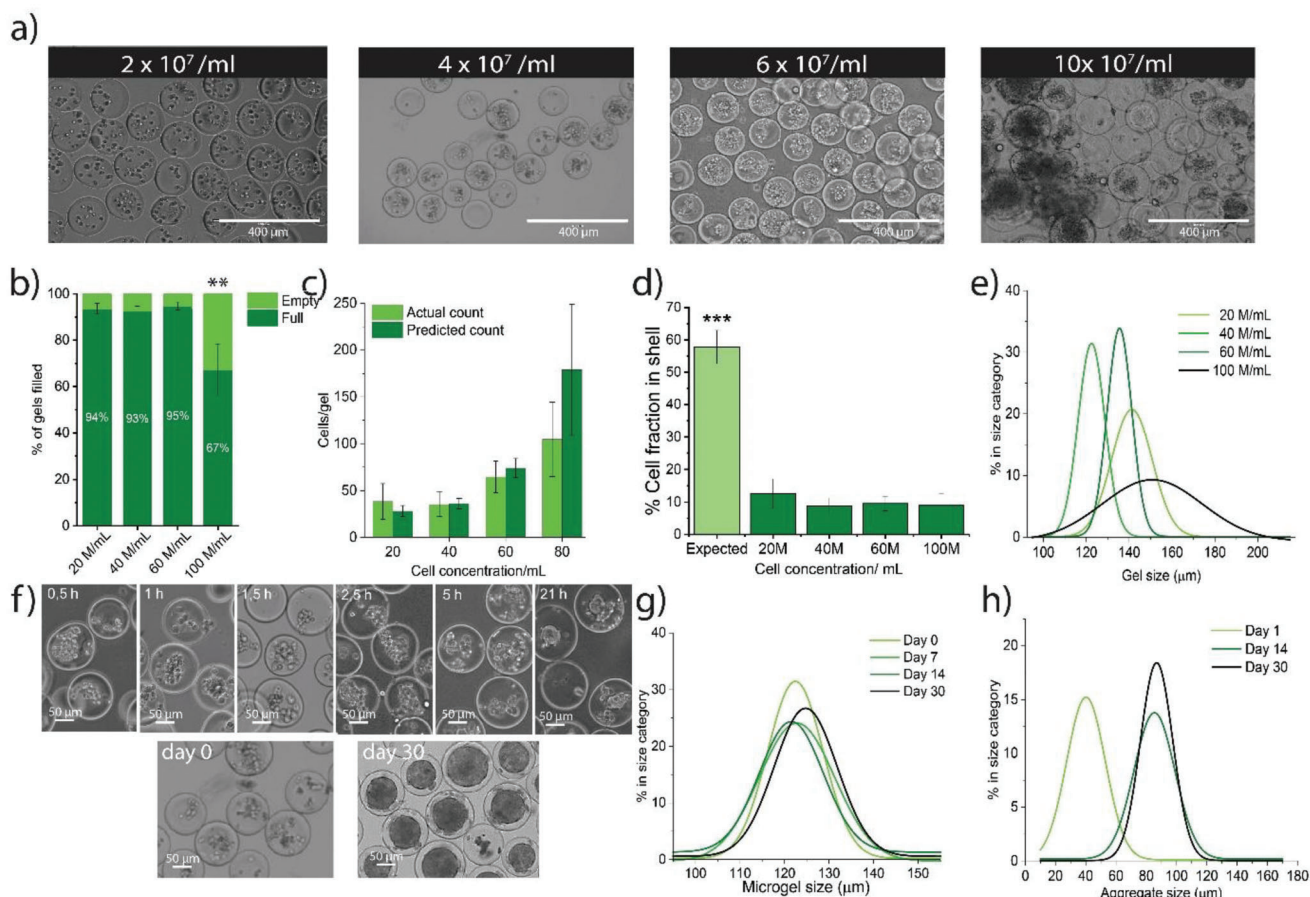


**Figure 4.** Optimization and parameter quantification of cell densities for efficient encapsulation of  $\beta$ -cells in hollow PEG-TA microgels. a) Brightfield micrographs of the four distinct cell densities tested for microencapsulation (20, 40, 60, and 100 million cells  $\text{mL}^{-1}$ ). b) Quantified encapsulation efficiency determined by the percentage of microgels containing cells. One-way ANOVA (\*\* $p < 0.005$ ). c) Quantification of the number of cells per microgel for the investigated densities. Number of cells/gel refers to the mean of the counted cells  $\pm$  SD. d) Quantification of the % of cell fraction located in the shell (one-way ANOVA, \*\*\* $p < 0.001$ ). e) Quantification of microgel size at investigated cell densities. f) Brightfield micrographs visualizing the  $\beta$ -cell aggregation process over a culture period of 21 h, and comparative brightfield micrographs of  $\beta$ -cell-laden microgels at the initial time point (day 0) and final time point of the experiments (day 30). g) Quantification of the cell-laden microgel and h) aggregate sizes over a 30-day culture period. (for each quantification,  $n \geq 100$  microgels/cells/spheroids).

immune activating properties that associate with the use of micromaterials.<sup>[24]</sup>

## 2.4. Microfluidic Production of $\beta$ -Cells Containing Hollow Microgels

In order to obtain information about the cell-density limitations of our microfluidic platform, cells of the  $\beta$ -cell line MIN6B1 were encapsulated at a flow speed of  $96 \mu\text{L min}^{-1}$  as a single cell suspension at distinct initial densities, and analyzed accordingly in order to obtain proper homogeneity of the cell-laden microgels without compromising the shape or integrity of the microgels. This cell line, derived from a mouse insulinoma is frequently used as a donor-independent  $\beta$ -cell model due to their ability to reproducibly respond to extracellular glucose challenges with measurable insulin secretion profiles, retaining the physiology of standard  $\beta$ -cells.<sup>[25]</sup> Four distinct initial cell densities were tested ( $2, 4, 6,$  and  $10 \times 10^7$  cells  $\text{mL}^{-1}$ ). Results suggested that there

was an optimal density interval to obtain optimal encapsulation efficiencies. Higher cell densities (e.g.,  $10 \times 10^7$  cells  $\text{mL}^{-1}$ ) resulted in heterogenous distributions of cells between the distinct microgels, which was associated with major cell clumping that also adversely affected microgel dispersity and size distribution. By using an initial pre-polymer suspension between 20 and 60 million  $\text{mL}^{-1}$ , homogenous monodispersity of microgels could be achieved with an encapsulation efficiency of  $>90\%$ , resulting in  $35\text{--}60 \pm 15$  cells per microgel. (Figure 4c).

$\approx 90\%$  of the encapsulated cells were centered and proliferative at the core compartment of the microgel, with only a small percentage of the cells ( $\approx 10\%$ ) becoming entrapped within the crosslinked shell. This can be regarded as a major issue and can potentially compromise the microgel integrity over time, although we could not identify significant burst of the microgels with cells integrated on the shell (Figure 4d). Microgel size was more heterogeneous at the higher cell densities, which was most likely due to the more granular character of the polymer-cell suspension at higher cell densities (Figure 4e).

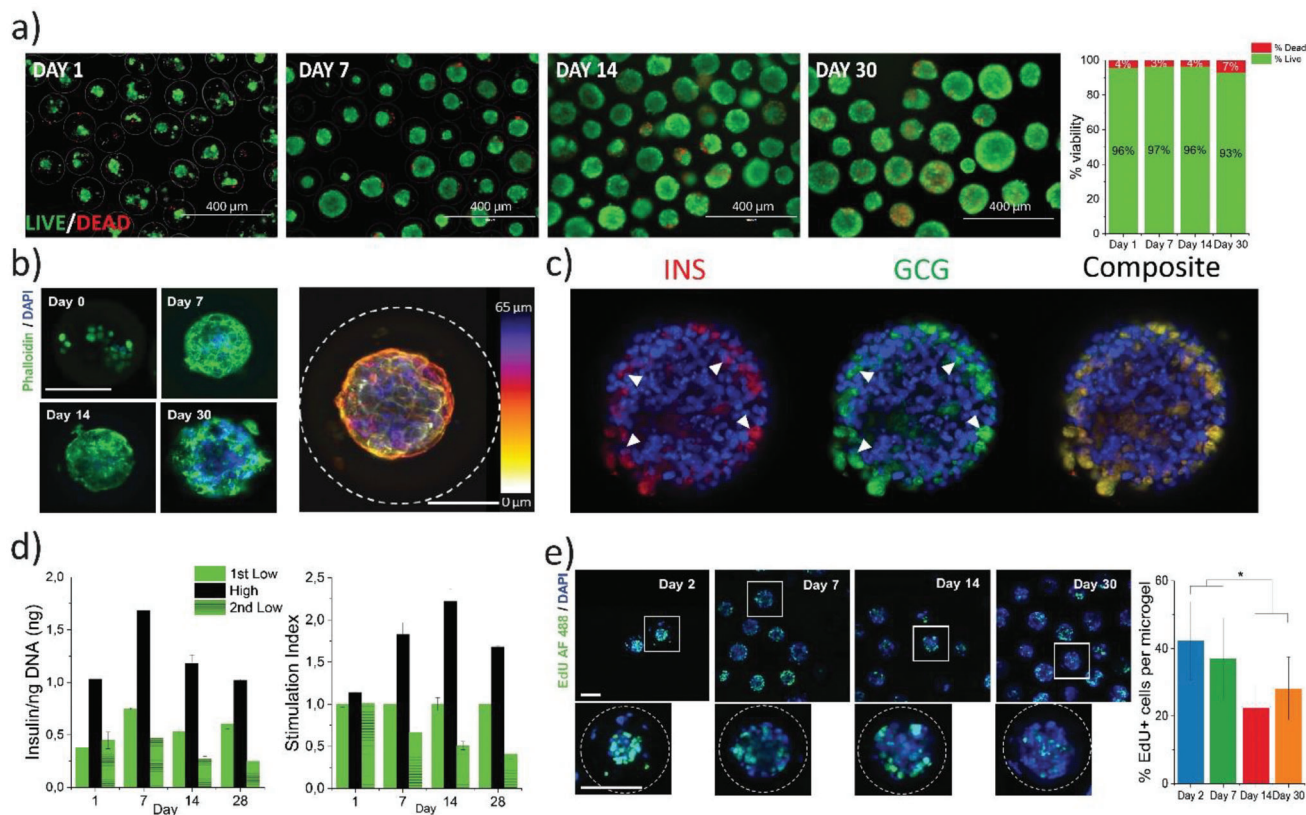


**Figure 5.** Encapsulated  $\beta$ -cells remain viable and functional within hollow PEG-TA microgels. a) Fluorescent micrographs of viable  $\beta$ -cell spheroids (live/dead staining) and respective semi-quantification of  $\beta$ -cell laden PEG-TA microgels over a period of 30 days ( $N > 50$ ). b)  $\beta$ -cell spheroids stained with phalloidin (green) and DAPI (blue) for the same period and respective height/depth measured. Scale bar 100  $\mu\text{m}$ . Height bar 65  $\mu\text{m}$ . c) Fluorescent confocal micrographs of encapsulated  $\beta$ -cell spheroid immunohistochemically stained for insulin (INS—red) and glucagon (GCG—green). Scale bar 100  $\mu\text{m}$ . d) Glucose-stimulated insulin secretion normalized to the total DNA content, and stimulation index (SI) of the microencapsulated cells for a period of 28 days. e) Fluorescent confocal micrographs and quantification of EDU stained cells that were microencapsulated for up to 30 days; Cells were stained with EDU (green) and DAPI (blue).  $N = 20$  aggregates measured for each time point. Scale bar 100  $\mu\text{m}$ .

Immediately after encapsulation, small clumps of cells were visible throughout the first 5 h post-encapsulation, eventually aggregating into a single spherical aggregate per microgel in less than 21 h (Figure 4f). The encapsulated cell spheroids continued to increase in size over a period of 30 days, eventually reaching a plateau of 80–100  $\mu\text{m}$  diameter where the entire microgel cavity became filled with a single spheroid, which slightly stretched of the microgel to a maximum of  $\approx 5 \mu\text{m}$  without significant breakage of microgels (Figure 4g). Advantageously, this thus allows for the consistent and reproducible production of monodisperse cellular spheroids, which is a feat that is not readily achievable in conventional aggregate-forming platforms such as hydrophobic surfaces and microwells. Based on the encapsulation efficiency, handleability, and microaggregation process, 40 million  $\text{mL}^{-1}$  cell density was selected as an optimal cell density to continue with further in vitro analysis.

## 2.5. Immunoprotected $\beta$ -Cells Remain Viable and Functional In Vitro

Microencapsulated cells were then studied in vitro for their ability to remain viable and respond to glucose. Within 24 post-

encapsulation, cells had aggregated into full 3D spheroids, which continued to proliferate throughout the entire duration of the experiment (30 days) with neglectable amounts of cell death ( $< 5\%$ ). (Figure 5a,b). These full-grown  $\beta$ -cell spheroids were capable of exhibiting both insulinoma cell markers insulin and glucagon inside of the microgel indicating maintained functionality (Figure 5c). This functionality was corroborated by a glucose-stimulated insulin secretion experiment, in which it was confirmed that the encapsulated spheroids were capable of adjusting insulin secretion in response to a low-high-low glucose challenge. The glucose stimulation index (SI) indicated that microencapsulated cells maintained their glucose responsiveness for at least 28 days (Figure 5d), although there was a slight decrease in the SI at the latter time point (Figure 5e). We hypothesize that the hollow microgels can also act as a physical barrier to control cell proliferation, which was supported by the observable reduction in the amount of EDU+ cells over time ( $\approx 50\%$  reduction from day 7 onward) (Figure 5f). Regardless, low levels of cell proliferation were still observed after 30 days of culture, which occurred at a level that matched the cell death thus likely being attributable to natural cellular turnover.



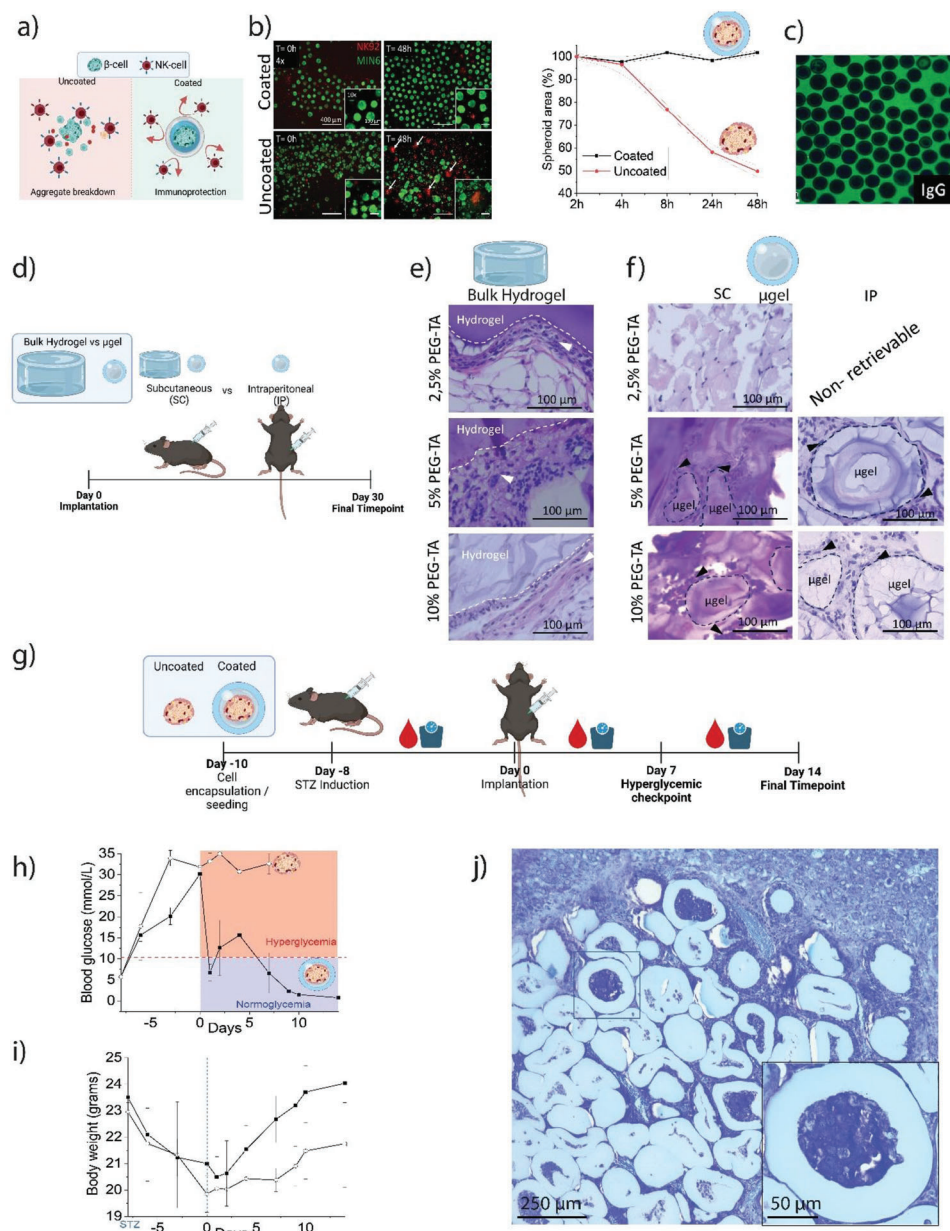


**Figure 6.** PEG-TA microgels provide non-immunogenic physical immunoisolation to  $\beta$ -cells that can function as living insulin delivery systems. a) Schematic depicting  $\beta$ -cell laden immunoprotection from NK-cell action. b) Fluorescence pictures of the co-incubation of both coated and non-coated CellTracker Green labeled MIN6 aggregates with CellTracker Red-labeled NK-92 cells and respective quantification based on spheroid area ( $N > 50$  quantified aggregates per condition). White arrows point to aggregate breakdown by NK92 action. c) Fluorescent confocal micrographs of cell laden microgels submerged in IgG-FITC (MW: 150 kDa) to confirm the microgels' immunoprotective properties when containing cells. d) Schematic depiction of the implantation site study (IP, intraperitoneal; SC, subcutaneous) with bulk hydrogels versus hollow microgels, displaying. e) Histological micrographs of SC implantation of the 2.5%, 5%, and 10% PEG-TA bulk hydrogels. White arrows indicate PFO tissue formation. f) Histological micrographs of SC and IP implantation of the hollow microgels with the same formulation same formulations. Black arrows indicate PFO tissue formation.  $N = 4$  mice per condition. g) IP implantation of  $\beta$ -laden microgels allowed for h) reestablishment of normoglycemia and i) weight recovery (versus non-encapsulated aggregates) within 5 days post-implantation and j) good tissue integration overall, showing alive spheroids at the moment of sacrifice.

## 2.6. PEG-TA Microgels Provide Non-Immunogenic Physical Immunoisolation to $\beta$ -Cells That Can Function as Living Insulin Delivery Systems

Following any biomaterial and xenogeneic cell implantation, NK-cells are involved in the first response to foreign materials and ca-

pable of producing cytokines and chemokines that can kill  $\beta$ -cells. We hypothesized that microencapsulating  $\beta$ -cells in microfluidically produced hollow PEG-TA microgel shield and protect  $\beta$ -cells from this cytotoxic NK-cell action<sup>[26]</sup> (Figure 6a). In order to test this hypothesis, we co-cultured encapsulated green-labeled MIN6 spheroids ( $>14$  days maturation in vitro, initial number  $\approx 50$  cells



per microgel), with red-labeled NK-92 cells for a period of 48 h. As expected, the diameter of the non-encapsulated control group significantly declined already after 8 h of culture, and continued to decline throughout the entire experiment indicating progressive cell death (Figure 6b). This coincided with a continuous increase in aggregates that disassembled into fragments. In contrast,  $\beta$ -cell aggregates within hollow PEG-TA microgels maintained their diameter and remained intact throughout the experiment, which coincided with little to no visible interaction with the co-cultured NK-cells. Similarly, the immunoprotective features of the  $\beta$ -cell-laden PEG-TA microgels were maintained for at least 30 days. This confirmed that neither the presence of the cells nor the observed cell spheroids induced stretching of the microgel adversely impacted the immunoprotective nature of the hollow PEG-TA microgels (Figure 6c).

We next investigated the immunogenicity of the material in immunocompetent mice. As material composition and implant size are known to affect immunogenicity in an independent manner, we implanted both hollow PEG-TA microgels and solid macro-sized bulk hydrogels. Specifically, microgels and bulk hydrogels using three formulations (2.5%, 5%, and 10%) were assessed on pericapsular fibrotic overgrowth (PFO). As implantation site-specific responses have been reported,<sup>[9]</sup> we implanted microgels both subcutaneously (SC) and intraperitoneally (IP) to uncover a potential implantation site-specific response to the microgels (Figure 6d–f). Results revealed overall higher (although mild) PFO formation and local immune cell activation (Figure S9, Supporting Information) in response to the microgels in comparison to the hydrogels, with no virtual differences between formulations. Fibrosis is indeed in many applications a major issue for the patency and long-term survival of cells in microcapsules. PFO, on the other hand, relies on several factors, including the size, material, and nanoroughness of the microcapsule. In numerous cases, this outcome is considered undesirable; however, it can also be seen as an integral part of the tissue response process, which ultimately facilitates revascularization. Uncontrolled fibrosis might interfere with revascularization and impede, for example, the development of a lymphatic system that drains inflammatory cells. Based on the histological analysis we have conducted, we have not observed any indications of excessive fibrosis. Based on the histological analysis we have conducted, we have not observed any indications of excessive fibrosis. We were able to detect the presence of vessels, and the capsules appear to remain intact. Moreover, SC implantation has proven to produce less PFO in comparison to IP implantation. Following these results, a preliminary implantation study was performed using encapsulated MIN6 $\beta$ 1 cells implanted subcutaneously in diabetic mice in an attempt to reestablish normoglycemia in 7 days with minimal impact on the fibrotic response. Results showed that although there was a mild immune response to the implanted microgels, as expected, implanted aggregates lost viability throughout the time of implantation, with histology showing significant encapsulated cell death (Figure S10, Supporting Information). This naturally did not produce any effect on the glucose levels. We hypothesized that the lack of vascularization leads to metabolic starvation of the encapsulated/implanted aggregates. Based on this data, IP implantation was selected as the implantation site of choice for the  $\beta$ -cell laden PEG-TA microgels.

We next investigated whether hollow PEG-TA microgels containing a  $\beta$ -cell aggregate could reestablish normoglycemia within a diabetic animal model. To this end, we surgically placed implants IP in STZ-induced mice in which we compared a group ( $n = 4$ ) of microencapsulated cellular spheroids (“coated”) versus a group ( $n = 4$ ) of pristine/non-encapsulated cellular spheroids (“uncoated”). A blood glucose checkpoint of 7 days was defined as a limit for the implanted mice to reach normoglycemia, due to ethical regulations. Interestingly, all mice that received  $\beta$ -cell aggregates containing microgels reached normoglycemia (blood glucose  $< 10 \text{ mmol L}^{-1}$ ) within 5 days, eventually even reaching hypoglycemic values after 14 days, mostly due to the tumoral character (e.g., continued proliferation and associated progressive increase  $\beta$ -cell mass) of the used cell line (Figure 6h). In contrast, non-encapsulated  $\beta$ -cells did not show any signs of recovering from hyperglycemia (blood glucose  $> 10 \text{ mmol L}^{-1}$ ) throughout 7 days and had to be euthanized. This further corroborated that the  $\beta$ -cells required immunoprotection and that PEG-TA was able to provide this protection for the length of this study (14 days). Similarly,  $\beta$ -cell spheroids within hollow PEG-TA microgels were able to fully restore the loss in body weight following STZ exposure, while pristine non-encapsulated  $\beta$ -cell spheroids were unable to achieve this feat (Figure 6i). Histology confirmed the presence of numerous intact aggregates at the moment of sacrifice of microencapsulated  $\beta$ -cells, while no trace was found of non-encapsulated  $\beta$ -cells (Figure 6j). Together, this data corroborated the in vitro data that PEG-TA microgels confer immunoprotection to encapsulated cells, which upon implantation allowed for the reestablishment of normoglycemic control in diabetic mice with enough PFO to allow the generation of vessels and maintain the integrity of the microgels. Furthermore, the implanted cells demonstrated the remarkable capability to promptly establish normoglycemia and sustain it over extended durations. This encouraging outcome suggests that the tissue response to the implanted cells was indeed favorable. Further investigations involving primary islet cells or differentiated iPSCs are imperative in combination with long-term (e.g., several months) to establish definitive conclusions regarding the enduring long-term clinical applicability and effectiveness of this material in the context of  $\beta$ -cell delivery.

Owing to the high nutrient and oxygen requirements of  $\beta$ -cells, achieving vascularization and consequent fast tissue integration is imperative to achieve a successful clinical outcome. In this scope, small microgels allow for fast nutrient diffusion to each of the islet-like spheroids. This is expected, as in previous studies we have reported that the use of smaller (e.g.,  $< 200 \mu\text{m}$ ) microgels associates with intimate integration within the (de novo) vascular network.<sup>[27,28]</sup> In contrast, larger microgels/devices (e.g.,  $> 500 \mu\text{m}$ ) commonly associate with insufficiently rapid vascularization, which poses a higher risk of encapsulated cell starvation.<sup>[29]</sup> Metabolic access is also affected by the location of implantation. In this manuscript, we explored various potential implantation sites such as subcutaneous space and intra-peritoneal cavity, which revealed that the implants in the highly vascularized intraperitoneal cavity achieved functionality with many visibly intact islet-like spheroids (Figure 6), while this observation was notably rarer in the lesser vascularized subcutaneous space (Figure S10, Supporting Information).

Additionally, the limited retrievability of microgels within the intraperitoneal cavity hindered more complete readouts from the histological analysis. Alternative encapsulation designs already tackle these types of issues, for example, by using wire and fiber-shaped zwitterionic alginate constructs to be able to facilitate retrievability,<sup>[30]</sup> although PFO is yet limitative for long-term implementation of these devices. We hypothesize that other types of solutions might be of interest without hindering the advantageous nature of using cell-laden microgels, such as using microporous annealed particles of PEG-TA microgels as a 3D scaffold for  $\beta$ -cell delivery.<sup>[31]</sup> Apart from enhanced retrievability compared to loose microgels, this type of geometry could potentially promote greater vascular ingrowth within the scaffold, at the same time mitigating the fibrotic outgrowth.

### 3. Conclusion

Here, we present a novel, non-immunogenic, immunoprotective, and bioinert material for effective shielding of  $\beta$ -cells from the host's immune response. By the adoption of a single-step outside-in enzymatic crosslinking strategy, we could reproducibly fabricate monodisperse micrometer-sized hollow PEG-TA microgels capable of harboring cells on a specialized microenvironment that allowed for efficient diffusion of nutrients, oxygen, glucose, and insulin, which supported  $\beta$ -cell function. In addition, the hollow PEG-TA microgels shielded the  $\beta$ -cells' from harmful interactions with the surrounding environment by eluding immune cell attack to implanted  $\beta$ -cells. The suitability of this hollow PEG-TA microgel for  $\beta$ -cell delivery was confirmed by implantation into diabetic mice, which reinstated normoglycemia within 7 days post-implantation in all implanted mice. In summary, these PEG-TA hollow microgels were proven to be suitable to act as insulin microreactors with great potential for  $\beta$ -cell delivery, which is anticipated to aid in the development of a treatment to aid humans suffering from type 1 diabetes.

### 4. Experimental Section

**Materials:** 8 arm polyethylene glycol (TP core) (Jankem Technology) Mw 20 kDa and 40 kDa, pyridine anhydrous (Sigma Aldrich), *N,N*-disuccinimidyl carbonate (Sigma Aldrich), TA 98% (Sigma Aldrich), dimethylformamide (DMF) anhydrous, diethyl ether (DEE), acetonitrile anhydrous, horse radish peroxidase 25 U g<sup>-1</sup> (Sigma Aldrich), hydrogen peroxide 30%, hexadecane (Sigma Aldrich), SPAN80. Fluorinated ethylene propylene tubing (FEP, inner diameter 500  $\mu$ m, outer diameter 1/16"), gastight syringes (Hamilton), and connectors were purchased from IDEX Health & Science. Borosilicate capillaries (inner diameter 700  $\mu$ m, outer diameter 870  $\mu$ m were purchased from CM Scientific. Silicone tubing (inner diameter 300  $\mu$ m, outer diameter 640  $\mu$ m, thickness 170  $\mu$ m) was obtained from Helix Medical. Triton X-100, phorbol-12-myristate-13-acetate (PMA), bovine serum albumin (BSA), and paraformaldehyde (PFA) were supplied from Sigma Aldrich. Fetal bovine serum (FBS), 0.25% trypsin/EDTA, RPMI 1640, 2-Mercaptoethanol (50 mM), Dulbecco's modified Eagle medium (DMEM), and penicillin/streptomycin were supplied by GIBCO. Mouse monoclonal anti-CD68 and goat anti-mouse AlexaFluor 647 were purchased from Abcam. Click-iT EdU Cell Proliferation Kit for Imaging, Alexa Fluor 488 dye was obtained from Thermo-Fisher Scientific. Phalloidin Alexa 488 was purchased from Invitrogen. Mouse Insulin ELISA was supplied by Mercodia.

**Ester Group Activation:** PEG-8arm 40 kDa (7.5 g, 1.5 mmol OH) was dissolved in 20 mL acetonitrile and treated with disuccinimidyl carbonate

(DSC) (0.76 g, 3.0 mmol) and pyridine (0.6 mL, 7.6 mmol). The mixed solution was stirred overnight at room temperature under argon. After that product was precipitated in a cold DEE and supernatant was removed. The residual solvent was evaporated under vacuum at room temperature. The product poly(ethylene glycol) succinimidyl carbonate (PEG-SC) was obtained as a white powder with a degree substitution with moieties of  $\approx$ 84%, 87%, and 95%, which were determined by HNMR.

**Functionalization of PEG-SC with TA:** To a solution of TA (500 mg, 0.441 mmol), a solution of PEG-SC ester 40 kDa (1.0 g, 0.19 mmol NHS) in dry DMF (3 mL) was added. The solution was stirred under argon for 4 h at 20 °C. The product was precipitated in DEE and dried under vacuum. The product was then dissolved in milliQ water and dialyzed (MWCO, 3500 g mol<sup>-1</sup>) against water. After dialysis product was freeze-dried and analyzed by HNMR in CDCl<sub>3</sub> NMR (ppm) = 7.26 (1H NMR of PEO-SC (400 MHz, CDCl<sub>3</sub>);  $\delta$  (ppm) = 2.84 (s, 4H), 3.62 (s, 3636H), 3.79 (t, 2H), 4.14 (t, 2H).

**8-arm Polyethylene Glycol Functionalization with TA Molecules:** In order to create an 8-arm PEG hydrogel in enzyme-mediated crosslinking reaction, the polymer arms were functionalized with a monophenolic molecule: TA. The functionalization procedure was composed of two steps. In the first step, ester groups were activated by using di-succinimidyl carbonate (DSC), providing an amine-reactive end group. In the second step, through amidation reaction, TA molecules were covalently coupled. The successful functionalization of 8  $\times$  PEG with DSC and with TA respectively, was confirmed by H-NMR which showed peaks as follows: 3.11 (NH-CH<sub>2</sub>, m, 8  $\times$  1H); 3.3–3.7 (EO, m, 3636H); 4.05 (CH<sub>2</sub>—O—C=O, 8  $\times$  2H); 6.6–6.75 and 6.9–7.07 (TA 2  $\times$  2H)

The degree of substitution (DS) with TA, calculated from the integral of peaks corresponding to two protons of TA and the integral of peaks corresponding to repetitive ethylene oxide unit, was between 87% and 100%. In addition, two molecular weights of 8  $\times$  PEG 20 and 40 kDa were functionalized with TA molecules, in order to test various hydrogel formulations.

**Hydrogel Disk/Microgel Fabrication and Characterization:** Polymer solutions of PEG-TA were made by dissolving polymer together with HRP in PBS overnight at room temperature. The HRP final concentration was 0.3 U mL<sup>-1</sup>. The range of polymer concentrations was prepared as follows: 2.5% w/v, 5% w/v, 10% w/v. In order to create the hydrogels, 0.3% hydrogen peroxide was added to polymer solutions and vortex for 3 s. The amount of added hydrogen peroxide was calculated as 0.5 equivalent of available phenolic groups, in order to obtain maximum density of crosslink density and consume all added hydrogen peroxide. The polymer solution was pipetted into a mold in order to form a hydrogel disk of 5  $\times$  2 mm size. Gelation time was obtained in vial test which was 16 s at room temperature. Next, the hydrogel disks were immersed in PBS overnight allowing for hydrogel swelling.

**Rheology:** Storage and loss modulus of hydrogel discs were measured on an Anton Paar Rheometer MCR by using a parallel plate geometry with a spindle size of 8 mm. All hydrogels were measured by applying a normal force of 0.005 N at room temperature. The measurement was carried out within a LVER (frequency  $f$  = 1 Hz, amplitude gamma 0.5%). For each hydrogel condition measurement was performed in triplicate ( $n$  = 3). The data points were recorded and desired values were calculated by the Anton Paar RheoCompass software.

**Swelling Degree of Hydrogel Discs:** PEG-TA hydrogel discs were immersed in PBS for 3 days, and swollen hydrogels (Ws) were weighed. Next, hydrogels were washed with milliQ water and dried under vacuum. Dried hydrogels (Wd) were weighed and swelling degree was calculated (Ws), and swelling degrees calculated by (%) = (Ws - Wd)/Wd  $\times$  100. Measurements were performed in triplicate ( $n$  = 3) for each condition.

**Microgel Fabrication:** The PMMA device used is described in ref. [19], fabricated using standard cutting and abrasion methods. Silica nozzles with 200  $\mu$ m of inner diameter were used on a flow focused setup and inserted on a transparent, semi-permeable silicone tubing to allow H<sub>2</sub>O<sub>2</sub> diffusion and subsequent crosslinking with the TA groups of the PEG-TA solution.

In short, PEG-TA supplemented 80 U mL<sup>-1</sup> HRP in PBS was emulsified in hexadecane with 3% SPAN80 by flow focusing. Next, microspheres were stabilized by flowing spheres via silicon tubing immersed in 30% hydrogen peroxide bath. Microgels were collected and emulsion was broken

by washing it with hexadecane. Microgels were spun down and oil was removed by washing with PBS until no oil was left. Next, microgels were resuspended in PBS. In order to confirm their size and shell thickness, microspheres were incubated with ethidium homodimer and analyzed by confocal microscope.

**Microgel Permeability:** Microgels were incubated with FITC-labeled proteins BSA (BSA—MW:66.5 kDa) and immunoglobulin G (IgG—MW:150 kDa) overnight. Following formulation of microgels were tested 20 kDa, polymer concentrations 2.5%, 5%, 10% w/v. The images of a microgels cross section were taken by a fluorescent microscope (Nikon confocal A1) and fluorescent intensity in the gels was quantified by using ImageJ, normalized to the intensity of the image background. 50 microgels per condition were analyzed.

**Cryo-FIB-SEM:** Organometallic platinum-based layer was deposited on microspheres PEGTA 20 kDa, polymer concentration 2.5%, 5%, 10% w/v. The microgels were immobilized at  $-150^{\circ}\text{C}$ , next temperature was raised to  $-90^{\circ}\text{C}$  and leaving the water to sublime. Surface of spheres was cut using a beam of Gallium ions. A cut of  $\approx 30\ \mu\text{m}$  was made. Images were taken using scanning electron microscope.

**Cell Culture:** Mouse insulinoma MIN6- $\beta 1$  cells were cultured in DMEM, supplemented with 10% (w/v) FBS,  $100\ \text{U mL}^{-1}$  Penicillin,  $100\ \text{mg mL}^{-1}$  Streptomycin (FisherScientific, USA), and  $71\ \text{mM}$  of  $\beta$ -mercaptoethanol (Gibco, ThermoFisher, USA). Media was changed every 2 days until 80% confluency was reached.

THP-1 monocytic cells were cultured in Roswell Park Memorial Institute 1640 (RPMI 1640, Gibco, ThermoFisher, USA) media, supplemented with 10% FBS, and 1% penicillin/streptomycin. In order to differentiate monocytes to macrophages,  $50\ \text{ng mL}^{-1}$  of phorbol-12-myristate-13-acetate (PMA) was added to the culture plate/flask for 14 h.

NK-92 cells were cultured in alpha-MEM media (with ribo- and deoxyribonucleosides), supplemented with 12.5% heat-inactivated FBS, 12.5% heat-inactivated horse serum,  $2\ \text{mM}$  L-Glutamine (Gibco, ThermoFisher, USA), 1% penicillin/streptomycin and  $150\ \text{U mL}^{-1}$  human IL-2 (Sigma Aldrich, St. Louis, USA)

All cell lines were maintained in a humidified environment at  $37^{\circ}\text{C}$  with 5%  $\text{CO}_2$ .

**Cell Encapsulation:** To microencapsulate MIN6 $\beta 1$  cell in PEG-TA microgels, the cells were washed twice with  $1\times$  PBS, trypsinized, flown through a  $40\ \mu\text{m}$  cell strainer, centrifuged, and resuspended in the distinct polymer solution (2.5%, 5%, 10% w/v) concentration solution to a density of  $4 \times 10^6\ \text{cells mL}^{-1}$ . 8% Optiprep was added to adjust the suspension density gradient to  $\rho = 1.05\ \text{g L}^{-1}$ . The cell/polymer suspension was then loaded onto a 1 mL gas-tight syringe (Hamilton), agitated, and put up on ice to avoid early cell clumping. Cell-laden microgels were formed and the resulting emulsion was broken by washing three or more times with surfactant-free n-hexadecane and a subsequent washing with  $1\times$  PBS, in order to get rid of the oil phase. The cell-laden gels were then maintained on the culture medium described above and media changed every 2 days until analysis. Cell viability of cell-laden hollow microgels was assessed by co-staining with calcein AM and ethidium homodimer-1 according to manufacturer's protocol (Invitrogen) and imaged using digital fluorescence microscopy (EVOS FL Imaging System, ThermoFisher). Quantification of cell count per gel at different densities was conducted using brightfield microscopy and analyzed with ImageJ on the day of encapsulation.  $N \geq 100$  microgels per density were examined.

Aggregate actin staining was performed using Phalloidin Alexa Fluor 488 after fixation on 4% PFA, permeabilization with 0,1% Triton X-100 and blocking with 1% BSA.

**Macrophage Phenotype Assessment by Immunofluorescence:** Immune cell activation assessment was achieved by co-culturing undifferentiated THP1 cells ( $5 \times 10^4\ \text{cells cm}^{-2}$ ) with hollow microgels on 48-well plated and fixed with 4% PFA at the time points of 24 and 72 h for immunofluorescence staining. Mouse monoclonal anti-CD80 (1:200, ab86473, Abcam) and Rabbit polyclonal anti-CD206 (1:100, ab64693, Abcam) were used as primary antibodies. AlexaFluor 647 Goat anti-mouse (1:200, ab150107, Abcam) and Alexa Fluor 488 donkey anti-rabbit (1:250, A11034, Invitrogen) were used as secondary antibodies. Semi-quantification of the activated cells was performed based on corrected total cell fluorescence

quantification (CTCF) of confocal pictures ( $n = 10$ ) using the following formula.

$$\text{CTCF} = \text{Total cell intensity} - (\text{cell size} \times \text{background intensity}) \quad (1)$$

**Macrophage Phenotype Assessment by qRT-PCR:** Prior to RNA extraction, PMA-differentiated THP1 cells ( $5 \times 10^4\ \text{cells cm}^{-2}$ ) were co-cultured with hollow microgels on 48-well plates and lysed using NucleoSpin RNA kit (Macherey-Nagel, Germany), following the protocol described by the supplier, to obtain the total RNA. About  $1\ \mu\text{g}$  RNA was used for synthesis using iScript cDNA Synthesis Kit (BIORAD, California, USA) following manufacturer's protocol. Obtained cDNA was used for RT-qPCR using SensiMix SYBR and Fluorescein Kit (Bioline, London, UK) on a CFX Connect Real-Time System (Bio-Rad, Hercules, California, USA). Primers for TNF $\alpha$  and IL1 $\beta$  genes were designed from specific DNA sequences available from NCBI (<https://www.ncbi.nlm.nih.gov/nucleore>) using PRIMER3plus (<http://www.bioinformatics.nl/cgi-bin/primer3plus/primer3plus.cgi>). Primer sequences were as follows: TNF- $\alpha$  sense TCCTTCAGACACCCCTCAACC; TNF- $\alpha$  antisense AGGCCCCAGTTTGAATCTT; IL1 $\beta$  sense GGGCTCAAGGAAAAGAATC; IL1 $\beta$  antisense TTCTGCTTGA-GAGGTGCTGA. All genes were normalized to the housekeeping reference gene GAPDH and data were presented as  $2^{-\Delta\Delta\text{Ct}}$ .

**Multiplex Immunoassay:** To perform multiplex immunoassay on whole blood exposed to PEG-TA microgels, blood from three distinct donors was collected using  $50\ \mu\text{g mL}^{-1}$  lepirudin as an anticoagulant into propylene tubes. For each condition, a solution of  $100\ \mu\text{L}$  of saline buffer (PBS containing  $\text{CaCl}_2$  and  $\text{MgCl}_2$ ) containing  $50\ \mu\text{L}$  of hollow microgels was co-incubated with  $500\ \mu\text{L}$  of whole blood for 30, 120, and 360 min at  $37^{\circ}\text{C}$  under constant agitation. Assay procedure details were followed as described in ref. [32]. Briefly, Complement activation in response to the microgels was stopped by addition of EDTA (10 mM) followed by centrifugation (3000 rpm for 15 min). Samples/supernatants were then stored at  $-80^{\circ}\text{C}$  for further use. LPS ( $100\ \text{ng mL}^{-1}$ ) was used as positive control to induce experimental sterile inflammation. Saline buffer and initial incubation time point considered ( $T = 0$ ) were used as a negative control to determine baseline levels of cytokines. After filtering the samples, aspecific heterophilic immunoglobulins were preabsorbed from those samples with Heteroblock (Omega Biologicals, Bozeman MT, USA). After the pretreatment, microgel samples were incubated with antibody-conjugated Mag-Plex microspheres for 1 h at room temperature with continuous shaking. The following steps were a 1-h incubation with biotinylated antibodies, and a 10 min incubation with phycoerythrin-conjugated streptavidin diluted in high performance ELISA buffer (HPE, Sanquin, the Netherlands). In between the different stages of the procedure, wash steps were integrated. Data acquisition was performed with FLEXMAP 3D equipment in combination with xPONENT software. Data was analyzed by 5-parametric curve fitting using Bio-Plex Manager software. All assays were performed at the ISO9001:2008 certified multiplex core facility of the laboratory of translational immunology of the university medical center Utrecht.

**Proliferation Immunofluorescence Analysis:** Proliferation analysis was done by adding  $10\ \mu\text{M}$  EdU to the culture medium on the day before the time point analysis (2, 7, 14, and 30 days). The staining procedure was performed according to the manufacturer's instructions; nuclei were counterstained with  $1\ \mu\text{g mL}^{-1}$  DAPI. Confocal micrographs were imaged using Nikon A1 confocal system and  $n = 15$  gels were analyzed.

**Glucose Induced Insulin Secretion Test:** Glucose-induced insulin secretion test was performed by cell-laden microgel incubation in Krebs buffer ( $115\ \text{mM NaCl}$ ,  $5\ \text{mM KCl}$ ,  $24\ \text{mM NaHCO}_3$ ,  $2.2\ \text{mM CaCl}_2$ ,  $20\ \text{mM HEPES}$ ,  $0.3\ \text{mM BSA}$ ,  $0.1\ \text{mM theophylline}$ , pH 7.4) containing high and low glucose concentrations (1.67 and 16.7 mM respectively). Insulin release was assessed by ELISA (Mercodia) according to the manufacturer's protocol. SI was calculated by dividing the average of each condition by the first low glucose condition. Insulin secretion was normalized to the total dsDNA content ( $\text{ng mL}^{-1}$ ) using the Quantifluor dsDNA kit (Promega, Madison, WI, USA) At least four replicates of each condition were used to obtain statistical significance.

**Microaggregate Formation Using Microwells:** Microaggregates used as a control for in vitro and in vivo experiments were created using the



same procedure described in Moreira-Teixeira et al.<sup>[33]</sup> In order to produce agarose micro-wells, 2% w/v ultrapure agarose (Invitrogen) was dissolved by heating in sterilized PBS and added drop by drop into a previously sterilized PDMS mold (with an area of 1.9 cm<sup>2</sup>), centrifuged to get rid of possible agarose bubbles and left to solidify for 1 h at 4 degrees. After solidifying, the gels with the negative-printed wells were detached from the mold and transferred into 24-well culture plates. Each well of the 24-well culture plate contains 4 × 10<sup>3</sup> micro-wells. In order to create microaggregates to act as a control for further experiments, MIN6B1 cells were trypsinized seeded at a density of 2.4 × 10<sup>4</sup> cells/well and maintained in culture until use.

**Study of  $\beta$ -Cell Spheroid and NK Cell Interaction:**  $\beta$ -cell spheroids were encapsulated as described above and kept in culture to mature for 10 days. NK-92 was simultaneously kept in culture until the day of the experiment. In parallel, non-encapsulated spheroids were seeded, matured in microwells as described above until reaching the same dimensions. Once matured ( $\approx$ 100  $\mu$ m in diameter), MIN6 spheroids were labeled with CellTracker Green CMFDA Dye (Invitrogen, catalog no. C2925), and NK-92 cells were labeled with CellTracker Red CMTPX Dye (Invitrogen, catalog no. C34552) at 37 °C for 30 min following manufacturer's protocol. Then, 50  $\mu$ L of microgels/aggregates were co-incubated with NK-92 cells (0.15 × 10<sup>6</sup> cells per well). Fluorescence micrographs were imaged using an EVOS FL microscope (Thermo Fisher, Waltham, USA) every 2 h for a period of 48 h. Quantification of the mean size of the spheroids was performed after image processing of the acquired fluorescence images using ImageJ ( $n$  = 10 images per time point).

**Animal/In Vivo Study:** Male C57BL/6NCRl mice weighing 22–25 grams were purchased from Charles River (Den Bosch, the Netherlands). Animals were housed at the central animal facility of the University of Groningen and maintained under 12-h light/dark cycles with ad libitum access to water and standard chow. All experiments were approved by both the local animal ethical committee of the University of Groningen and the national ethical commission for experimental animal use (#15168 and 185726). All surgical procedures were performed under general anesthesia with isoflurane (1.5% in 98.5% O<sub>2</sub>).

**Implantation Study:** To study site-specific tissue responses against the microgels, these were implanted subcutaneously and IP in non-diabetic mice ( $n$  = 4). For intraperitoneal implantation, a small incision was made in the skin and the abdominal muscle layer. The microcapsules suspended in Krebs-Ringer-Hepes (KRH; pH 7.4; 133 mM NaCl, 4.69 mM KCl, 1.18 mM KH<sub>2</sub>PO<sub>4</sub>, 1.18 mM MgSO<sub>4</sub>·7H<sub>2</sub>O, 25 mM HEPES, 2.52 mM CaCl<sub>2</sub>·2H<sub>2</sub>O) were injected via a syringe connected to a cannula. For subcutaneous implantation, a small incision was made in the skin and a subcutaneous pocket was created to place the microgels (resuspended in 500  $\mu$ L KRH buffer). The incisions were closed with a suture and the mice received one subcutaneous injection of buprenorphine (0.1 mg kg<sup>-1</sup>) to manage the pain. After 30 days these mice were sacrificed and the microgels were processed for histology.

**Induction of T1D Mellitus in Mice:** Diabetes was induced in the mice by a single intraperitoneal injection of STZ (Sigma Aldrich, the Netherlands; 200 mg kg<sup>-1</sup>, in 0.1 M citrate buffer, pH 4.5). Blood glucose measurements were obtained from tail vein blood using an Accu-check glucose meter (Ascensia Contour, Bayer, NJ, USA) and glucose test strips (Contour, Bayer, Switzerland). If diabetes was not established within 1 week (defined as blood glucose levels >20 mM), a second dose of STZ of 220 mg kg<sup>-1</sup> was administered. Mice were monitored at least twice a week for their glycemic state and weight.

**$\beta$ -Cell Transplantation into Diabetic Mice:** About 300  $\mu$ L of PEG-TA microgels laden with MIN6 $\beta$ 1 cells and uncoated  $\beta$ -cells were transplanted intraperitoneally into the diabetic mice ( $n$  = 4/group) as described for the implantation study. None of the recipients received immunosuppressive drugs before or after cell transplantation, but all mice received one subcutaneous injection of buprenorphine (0.1 mg kg<sup>-1</sup>) to manage the pain after transplantation. Graft rejection was defined as 2 consecutive blood glucose measurements above 20 mM.

**Histology:** Retrieved capsules were fixed in pre-cooled 2% PFA. This was replaced by 6% sucrose in PBS, and embedded in glycol methacrylate (GMA, Technovit 8100, Germany). The GMA-embedded capsules were sectioned at 2  $\mu$ m and processed for staining. The sections were stained

with toluidine blue solution and H&E stain to visualize and quantify capsules with cellular adhesion.

**Figures:** Schematics/cartoons were created using Biorender software (<https://biorender.com>)

**Statistical Analysis:** Experiments were carried out with at least three replicates for statistical analysis. All data are expressed as means  $\pm$  SD. Statistical significance was found using Origin(Pro)2019b. (OriginLab Corporation, Northampton, MA, USA) statistical software by Tukey's one-way ANOVA test with \* $p$  < 0.05, \*\* $p$  < 0.01, and \*\*\* $p$  < 0.001

## Supporting Information

Supporting Information is available from the Wiley Online Library or from the author.

## Acknowledgements

N.A.-G. and B.Z.L. Shared first authorship. This research was funded by JDRF (2-SRA-2018-684-S-B). J.L. acknowledges financial support from the Dutch Research Council (Vidi, 17522) and the European Research Council (starting grant, 759425).

## Conflict of Interest

The authors declare no conflict of interest.

## Data Availability Statement

The data that support the findings of this study are available from the corresponding author upon reasonable request.

## Keywords

$\beta$ -cell delivery, islet, microencapsulation, microfluidics, microgels, translational medicines, type I diabetes mellitus

Received: May 12, 2023

Revised: July 21, 2023

Published online:

- [1] A. L. McCall, *Endocrinol. Metab. Clin. North Am.* **2012**, *41*, 57.
- [2] a) A. R. Aroor, C. H. Mandavia, J. R. Sowers, *Heart Failure Clin.* **2012**, *8*, 609; b) A. M. Gomez-Perez, M. Damas-Fuentes, I. Cornejo-Pareja, F. J. Tinahones, *J. Clin. Med.* **2021**, *10*, 4497.
- [3] M. B. Haastrop, J. E. Henriksen, C. G. Mortz, C. Bindsløv-Jensen, *Clin. Transl. Allergy* **2018**, *8*, 35.
- [4] D. Russell-Jones, R. Khan, *Diabetes, Obes. Metab.* **2007**, *9*, 799.
- [5] S. Gentile, F. Strollo, A. Ceriello, A.-O. I. T. S. Group, *Diabetes Ther.* **2016**, *7*, 401.
- [6] K. M. Engebretsen, K. M. Kaczmarek, J. Morgan, J. S. Holger, *Clin. Toxicol.* **2011**, *49*, 277.
- [7] a) V. F. Duvivier-Kali, A. Omer, R. J. Parent, J. J. O'Neil, G. C. Weir, *Diabetes* **2001**, *50*, 1698; b) O. Korsgren, *Diabetes* **2017**, *66*, 1748; c) G. A. Paredes Juarez, M. Spasojevic, M. M. Faas, P. de Vos, *Front. Bioeng. Biotechnol.* **2014**, *2*, 26.
- [8] B. Kupikowska-Stobba, D. Lewińska, *Biomater. Sci.* **2020**, *8*, 1536.
- [9] J. Paez-Mayorga, I. Lukin, D. Emerich, P. de Vos, G. Orive, A. Grattoni, *Trends Pharmacol. Sci.* **2021**, *43*, 221,

- [10] C. L. Stabler, Y. Li, J. M. Stewart, B. G. Keselowsky, *Nat. Rev. Mater.* **2019**, *4*, 429.
- [11] R. W. Holdcraft, L. S. Gazda, L. Circle, H. Adkins, S. G. Harbeck, E. D. Meyer, M. A. Bautista, P. C. Martis, M. A. Laramore, H. V. Vinerean, R. D. Hall, B. H. Smith, *Cell Transplant.* **2014**, *23*, 929.
- [12] a) Z. Qi, C. Yamamoto, N. Imori, A. Kinukawa, K. C. Yang, G. Yanai, E. Ikenoue, Y. Shen, Y. Shirouzu, A. Hiura, K. Inoue, S. Sumi, *Cell Transplant.* **2012**, *21*, 525; b) Y. Teramura, Y. Kaneda, H. Iwata, *Biomaterials* **2007**, *28*, 4818.
- [13] a) N. Cohen, E. Toister, Y. Lati, M. Girshengorn, L. Levin, L. Silberstein, D. Seliktar, E. Epstein, *Cytotechnology* **2018**, *70*, 1075; b) S. Kizilel, A. Scavone, X. Liu, J. M. Nothias, D. Ostrega, P. Witkowski, M. Millis, *Tissue Eng., Part A* **2010**, *16*, 2217.
- [14] B. Li, L. Wang, F. Xu, X. Gang, U. Demirci, D. Wei, Y. Li, Y. Feng, D. Jia, Y. Zhou, *Acta Biomater.* **2015**, *22*, 59.
- [15] S. Saxena, C. E. Hansen, L. A. Lyon, *Acc. Chem. Res.* **2014**, *47*, 2426.
- [16] a) K. Alessandri, M. Feyeux, B. Gurchenkov, C. Delgado, A. Trushko, K. H. Krause, D. Vignjevic, P. Nassoy, A. Roux, *Lab Chip* **2016**, *16*, 1593; b) N. de Souza, *Nat. Methods* **2017**, *14*, 655.
- [17] A. Wojtuszczyński, M. Armanet, P. Morel, T. Berney, D. Bosco, *Diabetologia* **2008**, *51*, 1843.
- [18] A. Hirano, K. Shiraki, T. Arakawa, *Biopolymers* **2012**, *97*, 117.
- [19] B. van Loo, S. S. Salehi, S. Henke, A. Shamloo, T. Kamperman, M. Karperien, J. Leijten, *Mater. Today Bio* **2020**, *6*, 100047.
- [20] S. Henke, J. Leijten, E. Kemna, M. Neubauer, A. Fery, A. van den Berg, A. van Apeldoorn, M. Karperien, *Macromol. Biosci.* **2016**, *16*, 1524.
- [21] C. F. Guimarães, L. Gasperini, A. P. Marques, R. L. Reis, *Nat. Rev. Mater.* **2020**, *5*, 351.
- [22] J. M. de Rutte, J. Koh, D. Di Carlo, *Adv. Funct. Mater.* **2019**, *29*, 1900071.
- [23] T. Kamperman, B. van Loo, M. Gurian, S. Henke, M. Karperien, J. Leijten, *Lab Chip* **2019**, *19*, 1977.
- [24] O. Veiseh, J. C. Doloff, M. Ma, A. J. Vegas, H. H. Tam, A. R. Bader, J. Li, E. Langan, J. Wyckoff, W. S. Loo, S. Jhunjhunwala, A. Chiu, S. Siebert, K. Tang, J. Hollister-Lock, S. Aresta-Dasilva, M. Bochenek, J. Mendoza-Elias, Y. Wang, M. Qi, D. M. Lavin, M. Chen, N. Dholakia, R. Thakrar, I. Lacik, G. C. Weir, J. Oberholzer, D. L. Greiner, R. Langer, D. G. Anderson, *Nat. Mater.* **2015**, *14*, 643.
- [25] J.-I. Miyazaki, K. Araki, E. Yamato, H. Ikegami, T. Asano, Y. Shibasaki, Y. Oka, K.-I. Yamamura, *Endocrinology* **1990**, *127*, 126.
- [26] a) M. S. Massaro, R. Palek, J. Rosendorf, L. Cervenková, V. Liska, V. Moulisova, *Mater. Sci. Eng., C* **2021**, *127*, 112203; b) F. Wei, S. Liu, M. Chen, G. Tian, K. Zha, Z. Yang, S. Jiang, M. Li, X. Sui, Z. Chen, Q. Guo, *Front. Bioeng. Biotechnol.* **2021**, *9*, 664592.
- [27] Q. Liu, A. Chiu, L.-H. Wang, D. An, M. Zhong, A. M. Smink, B. J. de Haan, P. de Vos, K. Keane, A. Vegge, E. Y. Chen, W. Song, W. F. Liu, J. Flanders, C. Rescan, L. G. Grunnet, X. Wang, M. Ma, *Nat. Commun.* **2019**, *10*, 5262.
- [28] T. Kamperman, S. Henke, A. van den Berg, S. R. Shin, A. Tamayol, A. Khademhosseini, M. Karperien, J. Leijten, *Adv. Healthcare Mater.* **2017**, *6*, 1600913.
- [29] a) D. An, A. Chiu, J. A. Flanders, W. Song, D. Shou, Y.-C. Lu, L. G. Grunnet, L. Winkel, C. Ingvorsen, N. S. Christophersen, J. J. Fels, F. W. Sand, Y. Ji, L. Qi, Y. Pardo, D. Luo, M. Silberstein, J. Fan, M. Ma, *Proc. Natl. Acad. Sci. U. S. A.* **2018**, *115*, E263; b) A. J. Vegas, O. Veiseh, M. Gürtler, J. R. Millman, F. W. Pagliuca, A. R. Bader, J. C. Doloff, J. Li, M. Chen, K. Olejnik, H. H. Tam, S. Jhunjhunwala, E. Langan, S. Aresta-Dasilva, S. Gandham, J. J. McGarrigle, M. A. Bochenek, J. Hollister-Lock, J. Oberholzer, D. L. Greiner, G. C. Weir, D. A. Melton, R. Langer, D. G. Anderson, *Nat. Med.* **2016**, *22*, 306; c) O. Veiseh, J. C. Doloff, M. Ma, A. J. Vegas, H. H. Tam, Andrew R. Bader, J. Li, E. Langan, J. Wyckoff, W. S. Loo, S. Jhunjhunwala, A. Chiu, S. Siebert, K. Tang, J. Hollister-Lock, S. Aresta-Dasilva, M. Bochenek, J. Mendoza-Elias, Y. Wang, M. Qi, D. M. Lavin, M. Chen, N. Dholakia, R. Thakrar, I. Lacik, Gordon C. Weir, J. Oberholzer, D. L. Greiner, R. Langer, D. G. Anderson, *Nat. Mater.* **2015**, *14*, 643.
- [30] a) D. An, A. Chiu, J. A. Flanders, W. Song, D. Shou, Y. C. Lu, L. G. Grunnet, L. Winkel, C. Ingvorsen, N. S. Christophersen, J. J. Fels, F. W. Sand, Y. Ji, L. Qi, Y. Pardo, D. Luo, M. Silberstein, J. Fan, M. Ma, *Proc. Natl. Acad. Sci. U. S. A.* **2018**, *115*, E263; b) W. Liu, J. A. Flanders, L.-H. Wang, Q. Liu, D. T. Bowers, K. Wang, A. Chiu, X. Wang, A. U. Ernst, K. Shariati, J. S. Caserto, B. Parker, D. Gao, M. D. Plessner, L. G. Grunnet, C. Rescan, R. Pimentel Carletto, L. Winkel, J. M. Melero-Martin, M. Ma, *Small* **2022**, *18*, 2104899.
- [31] C. A. Roosa, M. Ma, P. Chhabra, K. Brayman, D. Griffin, *Adv. Ther.* **2022**, *5*, 2200064.
- [32] R. C. Scholman, B. Giovannone, S. Hiddingh, J. M. Meerding, B. Malvar Fernandez, M. E. A. van Dijk, M. J. Tempelman, B. J. Prakken, W. de Jager, *Cytokine* **2018**, *106*, 114.
- [33] L. S. Moreira Teixeira, J. C. Leijten, J. Sobral, R. Jin, A. A. van Apeldoorn, J. Feijen, C. van Blitterswijk, P. J. Dijkstra, M. Karperien, *Eur. Cells Mater.* **2012**, *23*, 387.